INFLUENCE OF SLIP CONDITION ON PERISTALTIC TRANSPORT OF A VISCOELASTIC FLUID WITH FRACTIONAL BURGERS' MODEL

by

Dharmendra TRIPATHI, Praveen Kumar GUPTA, and Subir DAS*

Department of Applied Mathematics, Institute of Technology,
Banaras Hindu University, Varanasi, India

Original scientific paper
UDC: 612.337:515.146:532.51
DOI: 10.2298/TSCI1102501T

The investigation is to explore the transportation of a viscoelastic fluid with fractional Burgers' model by peristalsis through a channel under the influence of wall slip condition. This analysis has been carried out under the assumption of long wavelength and low Reynolds number. An approximate analytical solution of the problem is obtained by using homotopy analysis method. It is assumed that the cross-section of the channel varies sinusoidally along the length of the channel. The expressions for axial velocity, volume flow rate, and pressure gradient are obtained. The effects of the fractional parameters α and β, material constants λ_1, λ_2, λ_3, slip parameter k, and amplitude ϕ on the pressure difference and friction force across one wavelength are discussed numerically and with the help of illustrations.

Key words: *peristalsis, fractional Burgers' fluid, pressure difference, friction force, homotopy analysis method*

Introduction

The transportation by which a fluid can be transported through a distensible tube when contraction or expansion waves propagate progressively along its length is known as peristaltic transport. The movements of food bolus through esophagus, chyme through intestines, urine in the ureters, and blood through blood vessels (arteries, veins, arterioles, venules, and capillaries *etc*.) are some examples of peristaltic flow. Studying peristaltic flows, especially with a view to applications in biomechanics and physiology, one should consider real material properties of the fluid being transported and determine the essential departures from the results of the theories for viscoelastic fluids. These investigations are, also, interesting for engineering applications.

* Corresponding author; e-mail: subir_das08@hotmail.com

Latham [1] investigated the fluid mechanics of peristaltic pumps and since then, other papers on the same subject have followed by Burns *et al*. [2] and Shapiro *et al*. [3]. These papers are useful contributions to the understanding of peristaltic pumping, but their relevance to the problem of the ureter is not investigated by the authors. Burns *et al*. [2] have used perturbation techniques to study the peristaltic motion through a channel and a tube, while Shapiro *et al*., have solved the problem of peristaltic pumping under assumption of long wavelength and low Reynolds number for two dimensional and axisymmetric flows of Newtonian fluid.

In many applications the flow pattern corresponds to a slip flow, the fluid presents a loss of adhesion at the wetted wall making the fluid slide along the wall. In the study of fluid-solid surface interactions the concept of slip of a fluid at a solid wall serves to describe macroscopic effects of certain molecular phenomena. In all study on peristaltic flow, much works are studied with no slip condition, but some few authors [4-7] have studied the wall slip effect on the peristaltic transport of Newtonian and non-Newtonian fluids through channel/tube.

In the literature, the mechanics of non-linear fluids presents special challenges to engineers, physicists and mathematicians since the non-linearity can manifest itself in a variety of ways. Some workers [8-10] are investigated the peristaltic transport of viscoelastic fluid with Maxwell model and they discussed the effect of relaxation time on the peristaltic transport. While Hayat *et al*. [11-13] have investigated the peristaltic transport of viscoelastic fluid with the Jeffrey model and they have also discussed the effect of relaxation and retardation time on the peristaltic transport.

Fractional calculus has encountered much success in the description of viscoelasticity. The starting point of the fractional derivative model of non-Newtonian model is usually a classical differential equation which is modified by replacing the time derivative of an integer order by the so-called Riemann–Liouville fractional calculus operators. This generalization allows one to define precisely non-integer order integrals or derivatives. Fractional Burgers' model is the model of viscoelastic fluid. In general, fractional Burgers' model is derived from well known Burgers' model by replacing the ordinary time derivatives to fractional order time derivatives and this plays an important role to study the valuable tool of viscoelastic properties. Some authors [14-28] have investigated unsteady flows of viscoelastic fluids with fractional Maxwell model, fractional generalized Maxwell model fractional second grade fluid, fractional Oldroyed-B model, fractional Burgers' model and fractional generalized Burgers' model through channel (annulus) tube and solutions for velocity field and the associated shear stress are obtained by using Laplace transform, Fourier transform, Weber transform, Hankel transform, and discrete Laplace transform.

First time, Liao [29] proposed the homotopy analysis method (HAM), which is a method to find series solutions of various types of linear and non-linear problem. HAM is based on homotopy and a fundamental concept of topology, has a freedom in choosing initial approximations and auxiliary linear operators which often helps to transfer the complicated non-linear problem to its simpler form. Recently some authors [30-35] have solved the linear and non-linear problem by using HAM.

Motivated by the above facts, in this paper the authors have studied the effects of wall slip condition on the peristaltic transport of viscoelastic fluid with fractional Burgers' model through a channel under the assumption of long-wavelength and low Reynolds number. HAM is applied to find approximate analytical solution of the problem and the numerical results of the problem for different particular cases are depicted graphically. The

effects of fractional parameters, material constants, slip parameter and amplitude on the pressure difference and friction force across one wavelength are discussed and presented through graphs.

Mathematical formulation

The constitutive equation for viscoelastic fluid with fractional Burgers' model is given by:

$$\left(1+\tilde{\lambda}_1^{\alpha}\frac{\partial^{\alpha}}{\partial\tilde{t}^{\alpha}}+\tilde{\lambda}_2^{\alpha}\frac{\partial^{2\alpha}}{\partial\tilde{t}^{2\alpha}}\right)\tilde{S}=\mu\left(1+\tilde{\lambda}_3^{\beta}\frac{\partial^{\beta}}{\partial\tilde{t}^{\beta}}\right)\dot{\gamma} \tag{1}$$

where $\tilde{t},\tilde{S},\dot{\gamma}$, and μ, are the time, shear stress, rate of shear strain, and viscosity, respectively, $\tilde{\lambda}_1,\tilde{\lambda}_2,\tilde{\lambda}_3$ are material constants, and α and β are the fractional time derivative parameters such that $0 < \alpha \le \beta \le 1$. This model reduces to fractional Oldroyd-B, fractional Maxwell, fractional second grade models, respectively, when, $\tilde{\lambda}_2=0,\tilde{\lambda}_2=\tilde{\lambda}_3=0,\tilde{\lambda}_1=\tilde{\lambda}_2=0$ and with $\alpha=\beta=1$, these models reduce to Oldroyd-B, Maxwell, second grade models. Classical Navier-Stokes model is obtained by substituting $\tilde{\lambda}_1=\tilde{\lambda}_2=\tilde{\lambda}_3=\tilde{\lambda}_4=0$.

The governing equations of motion for incompressible fluids are:

$$\begin{aligned}
\rho\left(\frac{\partial}{\partial\tilde{t}}+\tilde{u}\frac{\partial}{\partial\tilde{\xi}}+\tilde{v}\frac{\partial}{\partial\tilde{\eta}}\right)\tilde{u}&=-\frac{\partial\tilde{p}}{\partial\tilde{\xi}}+\frac{\partial\tilde{S}_{\tilde{\xi}\tilde{\xi}}}{\partial\tilde{\xi}}+\frac{\partial\tilde{S}_{\tilde{\xi}\tilde{\eta}}}{\partial\tilde{\eta}}\\
\rho\left(\frac{\partial}{\partial\tilde{t}}+\tilde{u}\frac{\partial}{\partial\tilde{\xi}}+\tilde{v}\frac{\partial}{\partial\tilde{\eta}}\right)\tilde{v}&=-\frac{\partial\tilde{p}}{\partial\tilde{\eta}}+\frac{\partial\tilde{S}_{\tilde{\eta}\tilde{\eta}}}{\partial\tilde{\eta}}+\frac{\partial\tilde{S}_{\tilde{\eta}\tilde{\xi}}}{\partial\tilde{\xi}}\\
\frac{\partial\tilde{u}}{\partial\tilde{\xi}}+\frac{\partial\tilde{v}}{\partial\tilde{\eta}}&=0
\end{aligned} \tag{2}$$

where $\rho,\tilde{u},\tilde{\xi},\tilde{v},\tilde{\eta}$, and $\tilde{p}$ are the fluid density, velocity, axial co-ordinate, transverse velocity, transverse co-ordinate, and pressure, respectively.

The physical parameters are non-dimensionalized as follows:

$$\begin{gathered}
\xi=\frac{\tilde{\xi}}{\lambda},\ \eta=\frac{\tilde{\eta}}{a},\ \lambda_1=\frac{c\tilde{\lambda}_1}{\lambda},\ \lambda_2=\frac{c\tilde{\lambda}_2}{\lambda},\ \lambda_3=\frac{c\tilde{\lambda}_3}{\lambda},\ t=\frac{c\tilde{t}}{\lambda},\ u=\frac{\tilde{u}}{c},\ v=\frac{\tilde{v}}{c\delta}\\
h=\frac{\tilde{h}}{a},\ \phi=\frac{\tilde{\phi}}{a},\ \delta=\frac{a}{\lambda},\ p=\frac{\tilde{p}a^2}{\mu c\lambda},\ Q=\frac{\tilde{Q}}{ac},\ S=\frac{a\tilde{S}}{\mu c},\ \mathrm{Re}=\frac{\rho ca\delta}{\mu}
\end{gathered} \tag{3}$$

where $\tilde{h},\tilde{\phi},\text{and}\,\tilde{Q}$ are transverse displacement of the walls, amplitude of the wave, and volume flow rate, respectively, and their counterparts without ~ are the corresponding parameters in the dimensionless form. The parameters λ, a, and c symbolize the wavelength, the semi-width of the channel, and the wave velocity, respectively. Re stands for the Reynolds number while δ is defined as the wave number.

Equations (2) with the help of eqs. (1) and (3) under the assumptions of long wavelength and low Reynolds number, give rise to:

$$\left(1+\lambda_1^{\alpha}\frac{\partial^{\alpha}}{\partial t^{\alpha}}+\lambda_2^{\alpha}\frac{\partial^{2\alpha}}{\partial t^{2\alpha}}\right)\frac{\partial p}{\partial \xi}=\left(1+\lambda_3^{\beta}\frac{\partial^{\beta}}{\partial t^{\beta}}\right)\left(\frac{\partial^2 u}{\partial \eta^2}\right)$$
$$\frac{\partial p}{\partial \eta}=0,\quad \frac{\partial u}{\partial \xi}+\frac{\partial v}{\partial \eta}=0 \tag{4}$$

The boundary conditions are:

– regularity condition
$$\frac{\partial u}{\partial \eta}=0 \quad \text{at} \quad \eta=0 \tag{5}$$

– slip condition
$$u=-k\frac{\partial u}{\partial \eta} \quad \text{at} \quad \eta=h \tag{6}$$

where k is the slip parameter,

$$\frac{\partial p}{\partial \xi}=p_0 \ \text{ at } \ t=0, \qquad \frac{\partial}{\partial t}\left(\frac{\partial p}{\partial \xi}\right)=p_1 \ \text{ at } \ t=0 \tag{7}$$

Integrating eq. (4) with respect to η, and using eq. (5), we get:

$$\left(1+\lambda_1^{\alpha}\frac{\partial^{\alpha}}{\partial t^{\alpha}}+\lambda_2^{\alpha}\frac{\partial^{2\alpha}}{\partial t^{2\alpha}}\right)\frac{\partial p}{\partial \xi}\eta=\left(1+\lambda_3^{\beta}\frac{\partial^{\beta}}{\partial t^{\beta}}\right)\left(\frac{\partial u}{\partial \eta}\right) \tag{8}$$

Further integrating eq. (8) from h to η and using eq. (6), yields:

$$\frac{1}{2}\left(1+\lambda_1^{\alpha}\frac{\partial^{\alpha}}{\partial t^{\alpha}}+\lambda_2^{\alpha}\frac{\partial^{2\alpha}}{\partial t^{2\alpha}}\right)\frac{\partial p}{\partial \xi}(\eta^2-h^2-2kh)=\left(1+\lambda_3^{\beta}\frac{\partial^{\beta}}{\partial t^{\beta}}\right)u \tag{9}$$

The volume flow rate is $Q=\int_0^h u\mathrm{d}\eta$, which, by virtue of eq. (9), reduces to:

$$-\frac{(h^3+3kh^2)}{3}\left(1+\lambda_1^{\alpha}\frac{\partial^{\alpha}}{\partial t^{\alpha}}+\lambda_2^{\alpha}\frac{\partial^{2\alpha}}{\partial t^{2\alpha}}\right)\frac{\partial p}{\partial \xi}=\left(1+\lambda_3^{\beta}\frac{\partial^{\beta}}{\partial t^{\beta}}\right)Q \tag{10}$$

The transformations between the wave and the laboratory frames, in the dimensionless form, are given by:

$$x=\xi-t,\ y=\eta,\ U=u-1,\ V=v,\ q=Q-h \tag{11}$$

where the left side parameters are in the wave frame and the right side parameters are in the laboratory frame.

We further assume that the wall undergoes contraction and relaxation as given by:

$$h=1-\phi\cos^2(\pi x) \tag{12}$$

The time-averaged flow rate $\bar{Q}$ is given by:

$$\bar{Q} = \int_0^1 Q\,\mathrm{d}t = \int_0^1 (q+h)\,\mathrm{d}t = q + 1 - \frac{\phi}{2} \tag{13}$$

Equation (10), in view of eqs. (11) and (13) gives:

$$\frac{\partial^{2\alpha}}{\partial t^{2\alpha}}\left(\frac{\partial p}{\partial x}\right) + \frac{\lambda_1^\alpha}{\lambda_2^\alpha}\frac{\partial^\alpha}{\partial t^\alpha}\left(\frac{\partial p}{\partial x}\right) + \frac{1}{\lambda_2^\alpha}\frac{\partial p}{\partial x} = -\frac{3}{\lambda_2^\alpha}\left(1 + \lambda_3^\beta \frac{\partial^\beta}{\partial t^\beta}\right)\left(\frac{\bar{Q} + h - 1 + \frac{\phi}{2}}{h^3 + 3kh^2}\right) \tag{14}$$

Solution of the problem by HAM

Equation (14) can be rewritten as:

$$\frac{\partial^{2\alpha} f}{\partial t^{2\alpha}} + \frac{\lambda_1^\alpha}{\lambda_2^\alpha}\frac{\partial^\alpha f}{\partial t^\alpha} + \frac{1}{\lambda_2^\alpha} f = \left(1 + \lambda_3^\beta \frac{\partial^\beta}{\partial t^\beta}\right) A \tag{15}$$

where $f(x,t) = \partial p/\partial x$ and $A = -(3/\lambda_2^\alpha)\{[\bar{Q} + h - 1 + (\phi/2)]/(h^3 + 3kh^2)\}$

To solve eq. (15) by means of HAM, we choose the initial approximation:

$$f_0(x,t) = p_0 + p_1 t \tag{16}$$

and the linear operator

$$L[\phi(x,t;\theta)] = \frac{\partial^{2\alpha}\phi(x,t;\theta)}{\partial t^{2\alpha}}, \quad 0 < a \le 1 \tag{17}$$

with the property

$$L[c_1 + c_2 t] = 0 \tag{18}$$

where c_1 and c_2 are integral constants. Furthermore, eq. (15) suggests that we define an equation of non-linear operator as:

$$N[\phi(x,t;\theta)] = \frac{\partial^{2\alpha}\phi(x,t;\theta)}{\partial t^{2\alpha}} + \frac{\lambda_1^\alpha}{\lambda_2^\alpha}\frac{\partial^\alpha \phi(x,t;\theta)}{\partial t^\alpha} + \frac{1}{\lambda_2^\alpha}\phi(x,t;\theta) - \left(1 + \lambda_3^\beta \frac{\partial^\beta}{\partial t^\beta}\right) A \tag{19}$$

Now, we construct the zero-order deformation equation:

$$(1-\theta)\,L[\phi(x,t;\theta) - Z_0(x,t)] = \theta \hbar\, N[\phi(x,t;\theta)] \tag{20}$$

Obviously, when $\theta = 0$ and $\theta = 1$,

$$\phi(x,t;0) = Z_0(x,t) = f_0(x,t) \quad \text{and} \quad \phi(x,t;1) = f(x,t) \tag{21}$$

Therefore, as the embedding parameter θ increases from zero to unity, $\phi(x,t,\theta)$ varies from the initial guess $f_0(x,t)$ to the solution $f(x,t)$. Expanding $\phi(x,t;\theta)$ in Taylor series with respect to θ, one can find:

$$\phi(x, t;\ \theta) = Z_0(x, t) + \sum_{m=1}^{\infty} Z_{\mathrm{m}}(x,\ t)\theta^m$$

where

$$Z_{\mathrm{m}}(x, t) = \frac{1}{m!}\frac{\partial^m \phi(x, t; \theta)}{\partial \theta^m}\bigg|_{\theta=0}$$

If the auxiliary linear operator, the initial guess and the auxiliary parameter $\hbar$ are properly chosen, the above series is convergent at $\theta = 1$, then one has:

$$f(x, t) = Z_0(x, t) + \sum_{m=1}^{\infty} Z_{\mathrm{m}}(x, t)$$

which must be one of the solutions of the original non-linear equation, as proved by Liao [36].

Now we define the vector:

$$\vec{Z}_n(x, t) = [Z_0(x, t), Z_1(x, t), ..., Z_{\mathrm{n}}(x, t)]$$

Then the m^{th}-order deformation equation is

$$L[Z_{\mathrm{m}}(x, t) - \chi_{\mathrm{m}}\, Z_{m-1}(x, t)] = \hbar\, R_{\mathrm{m}}[\vec{Z}_{m-1}(x, t)] \tag{22}$$

with the initial conditions

$$Z_{\mathrm{m}}(x, 0) = 0 \quad \text{and} \quad \frac{\partial Z_{\mathrm{m}}(x, 0)}{\partial t} = 0 \tag{23}$$

where

$$R_{\mathrm{m}}[\vec{Z}_{m-1}(x, \tau)] = D_t^{2\alpha}(Z_{m-1}) + \frac{\lambda_1^{\alpha}}{\lambda_2^{\alpha}} D_t^{\alpha}(Z_{m-1}) + \frac{1}{\lambda_2^{\alpha}} Z_{m-1} - \left(1 + \lambda_3^{\beta}\frac{\partial^{\beta}}{\partial t^{\beta}}\right) A, \tag{24}$$

and $\chi_{\mathrm{m}} = \begin{cases} 0, & m \le 1, \\ 1, & m > 1. \end{cases}$

Now, the solution of the m^{th}-order deformation eq. (22) for $m \ge 1$, becomes:

$$Z_{\mathrm{m}}(x, t) = \chi_{\mathrm{m}}\, Z_{m-1}(x, t) + \hbar\, J_t^{2\alpha}\{R_{\mathrm{m}}[\vec{Z}_{m-1}(x, t)]\mathrm{d}t\} + c_1 + c_2 t \tag{25}$$

where the integration constants c_1 and c_2 are determined by the initial condition (23). We now successively obtain:

$$Z_1(x, t) = \frac{\hbar\lambda_1^{\alpha} p_1}{\lambda_2^{\alpha}}\frac{t^{\alpha+1}}{\Gamma(\alpha+2)} + \hbar\left(\frac{p_0}{\lambda_2^{\alpha}} - A\right)\frac{t^{2\alpha}}{\Gamma(2\alpha+1)} + \hbar\frac{p_1}{\lambda_2^{\alpha}}\frac{t^{2\alpha+1}}{\Gamma(2\alpha+2)} - \hbar A\lambda_3^{\beta}\frac{t^{2\alpha-\beta}}{\Gamma(2\alpha-\beta+1)} \tag{26}$$

$$Z_2(x,t)=\hbar(\hbar+1)\frac{\lambda_1^{\alpha}p_1}{\lambda_2^{\alpha}}\frac{t^{\alpha+1}}{\Gamma(\alpha+2)}+\hbar\left(\frac{(\hbar+1)p_0}{\lambda_2^{\alpha}}-(\hbar+2)A\right)\frac{t^{2\alpha}}{\Gamma(2\alpha+1)}+$$
$$+\hbar\left(\frac{\hbar\lambda_1^{2\alpha}}{\lambda_2^{\alpha}}+\hbar+1\right)\frac{p_1}{\lambda_2^{\alpha}}\frac{t^{2\alpha+1}}{\Gamma(2\alpha+2)}-\hbar(\hbar+2)A\lambda_3^{\beta}\frac{t^{2\alpha-\beta}}{\Gamma(2\alpha-\beta+1)}+$$
$$+\hbar^2\frac{\lambda_1^{\alpha}}{\lambda_2^{\alpha}}\left(\frac{p_0}{\lambda_2^{\alpha}}-A\right)\frac{t^{3\alpha}}{\Gamma(3\alpha+1)}+2\hbar^2\frac{\lambda_1^{\alpha}}{\lambda_2^{2\alpha}}p_1\frac{t^{3\alpha+1}}{\Gamma(3\alpha+2)}-$$
$$-\hbar^2A\frac{\lambda_1^{\alpha}\lambda_3^{\beta}}{\lambda_2^{\alpha}}\frac{t^{3\alpha-\beta}}{\Gamma(3\alpha-\beta+1)}+\frac{\hbar^2}{\lambda_2^{\alpha}}\left(\frac{p_0}{\lambda_2^{\alpha}}-A\right)\frac{t^{4\alpha}}{\Gamma(4\alpha+1)}+\hbar^2\frac{p_1}{\lambda_2^{2\alpha}}\frac{t^{4\alpha+1}}{\Gamma(4\alpha+2)}-$$
$$-\hbar^2A\frac{\lambda_3^{\beta}}{\lambda_2^{\alpha}}\frac{t^{4\alpha-\beta}}{\Gamma(4\alpha-\beta+1)} \tag{27}$$

$$Z_3(x,t)=\hbar(\hbar+1)^2\frac{\lambda_1^{\alpha}p_1}{\lambda_2^{\alpha}}\frac{t^{\alpha+1}}{\Gamma(\alpha+2)}+\hbar\left(\frac{(\hbar+1)^2p_0}{\lambda_2^{\alpha}}-(\hbar^2+3\hbar+3)A\right)\frac{t^{2\alpha}}{\Gamma(2\alpha+1)}+$$
$$+\hbar(\hbar+1)\left(\frac{2\hbar h\lambda_1^{2\alpha}}{\lambda_2^{\alpha}}+\hbar+1\right)\frac{p_1}{\lambda_2^{\alpha}}\frac{t^{2\alpha+1}}{\Gamma(2\alpha+2)}-\hbar(\hbar^2+3\hbar+3)A\lambda_3^{\beta}\frac{t^{2\alpha-\beta}}{\Gamma(2\alpha-\beta+1)}+$$
$$+\hbar^2\frac{\lambda_1^{\alpha}}{\lambda_2^{\alpha}}\left(\frac{2(\hbar+1)p_0}{\lambda_2^{\alpha}}-A(2\hbar+3)\right)\frac{t^{3\alpha}}{\Gamma(3\alpha+1)}+\hbar^2\frac{\lambda_1^{\alpha}}{\lambda_2^{2\alpha}}p_1\left(\frac{\hbar\lambda_1^{2\alpha}}{\lambda_2^{\alpha}}+4(\hbar+1)\right)\frac{t^{3\alpha+1}}{\Gamma(3\alpha+2)}-$$
$$-\hbar^2(2\hbar+3)A\frac{\lambda_1^{\alpha}\lambda_3^{\beta}}{\lambda_2^{\alpha}}\frac{t^{3\alpha-\beta}}{\Gamma(3\alpha-\beta+1)}+$$
$$+\frac{\hbar^2}{\lambda_2^{\alpha}}\left(\frac{\hbar\lambda_1^{2\alpha}p_0}{\lambda_2^{2\alpha}}+\frac{2(\hbar+1)}{\lambda_2^{\alpha}}p_0-A\hbar\frac{\lambda_1^{2\alpha}}{\lambda_2^{\alpha}}-A(2\hbar+3)\right)\frac{t^{4\alpha}}{\Gamma(4\alpha+1)}+$$
$$+\hbar^2\frac{p_1}{\lambda_2^{2\alpha}}\left(3\hbar\frac{\lambda_1^{2\alpha}}{\lambda_2^{\alpha}}+2(\hbar+1)\right)\frac{t^{4\alpha+1}}{\Gamma(4\alpha+2)}-\hbar^2A\frac{\lambda_3^{\beta}}{\lambda_2^{\alpha}}(\hbar\lambda_1^{2\alpha}+2\hbar+3)\frac{t^{4\alpha-\beta}}{\Gamma(4\alpha-\beta+1)}-$$
$$-2\hbar^3\frac{\lambda_1^{\alpha}}{\lambda_2^{2\alpha}}\left(\frac{p_0}{\lambda_2^{\alpha}}-A\right)\frac{t^{5\alpha}}{\Gamma(5\alpha+1)}+3\hbar^3p_1\frac{\lambda_1^{\alpha}}{\lambda_2^{3\alpha}}\frac{t^{5\alpha+1}}{\Gamma(5\alpha+2)}-2\hbar^3A\frac{\lambda_1^{\alpha}\lambda_3^{\beta}}{\lambda_2^{2\alpha}}\frac{t^{5\alpha-\beta}}{\Gamma(5\alpha-\beta+1)}+$$
$$+\frac{\hbar^3}{\lambda_2^{2\alpha}}\left(\frac{p_0}{\lambda_2^{\alpha}}-A\right)\frac{t^{6\alpha}}{\Gamma(6\alpha+1)}+\frac{\hbar^3}{\lambda_2^{3\alpha}}p_1\frac{t^{6\alpha+1}}{\Gamma(6\alpha+2)}-\frac{\hbar^3A\lambda_3^{\beta}}{\lambda_2^{2\alpha}}\frac{t^{6\alpha-\beta}}{\Gamma(6\alpha-\beta+1)} \tag{28}$$

as so on.

Proceeding in this manner the components Z_n, $n \geq 0$ of the HAM can be completely obtained and the series solutions are thus entirely determined.

Finally we approximate the analytical solution $f(x,t)$ by the truncated series:

$$f(x,t)=\lim_{N\to\infty}\Phi_N(x,t) \tag{29}$$

where

$$\Phi_N(x,t)=\sum_{n=0}^{N-1}Z_n(x,t)$$

The above series solutions generally converge very rapidly. A classical approach of convergence of this type of series is already presented by Abbaoui *et al.* [37].

The pressure difference Δp and friction force F across one wavelength are given by:

$$\Delta p = \int_0^1 \frac{\partial p}{\partial x} \mathrm{d}x \tag{30}$$

$$F = \int_0^1 \left(-h \frac{\partial p}{\partial x} \right) \mathrm{d}x \tag{31}$$

Numerical results and discussion

The main objective of this article is to study the influences of wall slip condition and characteristics of peristaltic pumping of fractional Burgers' fluid through the channel. Equations (30) and (31) are not integrable analytically due to the complexity of the expressions (26)-(28). Consequently, numerical integration is required to evaluate the integral and hence MATHEMATICA software is used to evaluate the integrals and later generate all the plots.

Numerical and graphical results are described just to see the effects of various fractional time derivative parameters α and β, material constants λ_1, λ_2, λ_3, and λ_4, time t and amplitude ϕ on the pressure rise Δp and friction force F through a channel. The behaviors of different models of viscoelastic fluids such as fractional Burgers' model (FBM), fractional Oldroyed-B model (FOBM), fractional Maxwell model (FMM), fractional second grade model (FSGM), second grade model (SGM) on Δp and F are presented through illustrations.

Figures 1-24 are sketched to see the variations of pressure rise Δp and friction forces F against averaged flow rate $\bar{Q}$, at fixed value of $p_0 = 0$ and $p_1 = 0$. As expected there is a linear relation between pressure rise and averaged flow rate. Also it is worth mentioning that the increase in the averaged flow rate reduces the pressure and thus maximum flow rate is achieved at zero pressure and maximum pressure occurs at zero averaged flow rate. Through figs. 1-8, we discuss the effects of relevant parameters on pressure rise with averaged flow rate. The influences of same parameters on the friction force *vs.* averaged flow rate are presented in figs. 9-16. Figures 17-24 display the comparative study for different models of fluids on pressure rise with averaged flow rate.

Figures 1-8 are plotted in order to see the effects of the parameters on the variation of pressure rise against the averaged flow rate. Figure 1 illustrates the variation of Δp *vs.* the averaged flow rate $\bar{Q}$ for different values of α = 1/5, 2/5, 3/5, 4/5 at fixed parameters ϕ = 0.6, k = 1, t = 0.4, β = 4/5, λ_1 = 4, λ_2 = 1, λ_3 =1. Figure 2 depicts that Δp *vs.* the averaged flow rate $\bar{Q}$, for various values of β = 1/5, 2/5, 3/5, 4/5 at fixed parameters ϕ = 0.6, k = 1, t = 0.4, α = = 1/5, λ_1 = 4, λ_2 = 1, and λ_3 =1. It is evident that the pressure decreases with increase in α while it increases with increase in β. In order to illustrate the effects of material constants λ_1 = 4, 3, 2, and 1, λ_2 = = 0.4, 0.6, 0.8, and 1.0, λ_3 = 4, 3, 2, and 1 on the pressure rise against averaged flow rate. Figures 3-5 have been prepared at fixed parameters ϕ = 0.6, k = 1, t = 0.4, α = 1/5, and β = 4/5. It is seen that pressure rise increases by increasing λ_1 whereas decreases with the increase in λ_2 and the effect of λ_3 is found similar to that of λ_1. Figure 6 presents the variation of pressure with averaged flow rate for various values of slip parameter k = 0, 1, 2, and 3 at fixed parameters ϕ = 0.6, t = 0.4, α = 1/5, β = 4/5, λ_1 = 4, λ_2 = 1, and λ_3 = 1. It is interesting to note that with an increase in k, pressure rise diminishes. Figure 7 and 8 display the influence of time t and amplitude ϕ = 0.4, 0.5, 0.6, and 0.7 on pressure with averaged flow rate at k = 1, α = = 1/5, β = 4/5, λ_1 = 4, λ_2 = 1, and λ_3 = 1. The observations regarding the effects t and ϕ on pressure rise are similar to that of β.

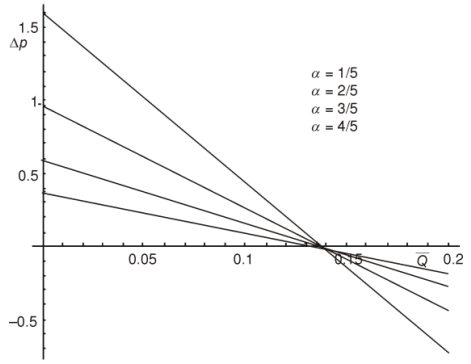

Figure 1. Pressure *vs.* averaged flow rate for various values of α at ϕ = 0.6, k = 1, t = 0.4, β = 4.5, λ_1, = 4, λ_2 = 1, and λ_3 = 1

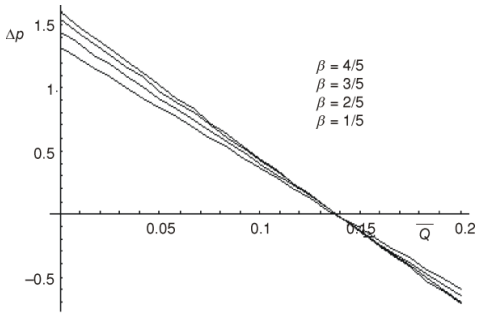

Figure 2. Pressure *vs.* averaged flow rate for various values of β at ϕ = 0.6, k = 1, t = 0.4, α = 1/5, λ_1 = 4, λ_2 = 1, and λ_3 = 1

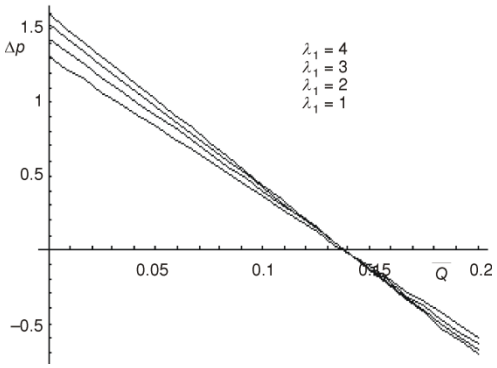

Figure 3. Pressure *vs.* averaged flow rate for various values of λ_1 at ϕ = 0.6, k = 1, t = 0.4, α = 4.5, and β = 4/5

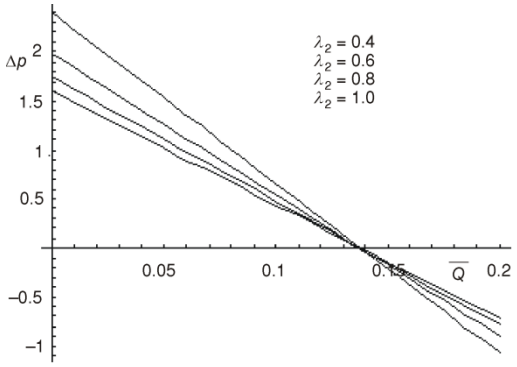

Figure 4. Pressure *vs.* averaged flow rate for various values of λ_2 at ϕ = 0.6, k = 1, t = 0.4, α = 1.5, β = 4/5, λ_1, = 4, and λ_3 = 1

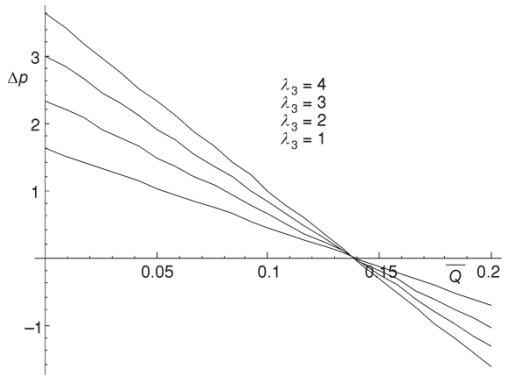

Figure 5. Pressure *vs.* averaged flow rate for various values of λ_2 at ϕ = 0.6, k = 1, t = 0.4, α = 1.5, β = 4/5, λ_1, = 4, and λ_2 = 1

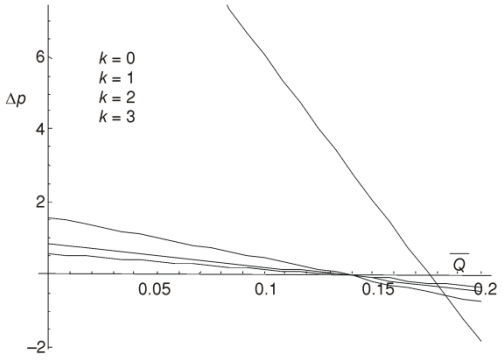

Figure 6. Pressure *vs.* averaged flow rate for various values of k at ϕ = 0.6, k = 1, t = 0.4, α = 1.5, β = 4/5, λ_1, = 4, λ_2 = 1, and λ_3 = 1

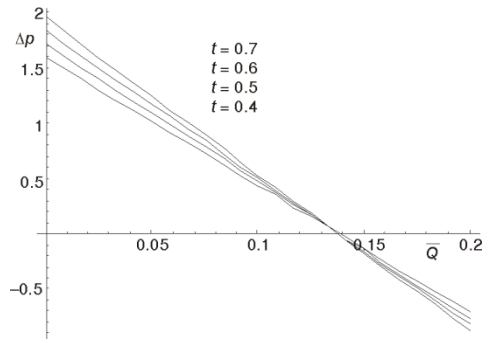

Figure 7. Pressure *vs.* averaged flow rate for various values of t at $\phi = 0.6$, $k = 1$, $\alpha = 1.5$, $\beta = 4/5$, $\lambda_1 = 4$, $\lambda_2 = 1$, and $\lambda_3 = 1$

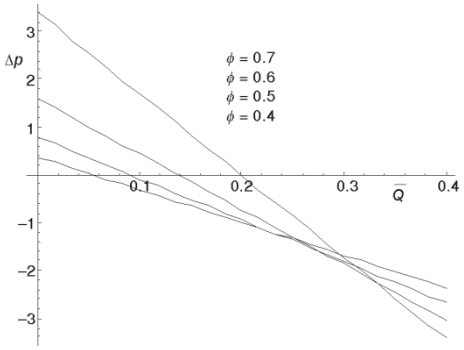

Figure 8. Pressure *vs.* averaged flow rate for various values of of ϕ at $t = 0.4$, $k = 1$, $\alpha = 1.5$, $\beta = 4/5$, $\lambda_1 = 4$, $\lambda_2 = 1$, and $\lambda_3 = 1$

Figures 9-16 show the effects of relevance of parameters on friction force F with $\bar{Q}$. Figures 9-10 describe the results obtained for F *vs.* $\bar{Q}$ at various values of α and β. Figures 11-14 are plotted to show the influences of material constants λ_1, λ_2, and λ_3 on the variation of F with $\bar{Q}$. Also the variations of F with $\bar{Q}$ for different values of t and ϕ are presented in figs. 15 and 16, respectively. From figs. 9-16, it is revealed that the friction force has the opposite behavior compared to that of the pressure rise.

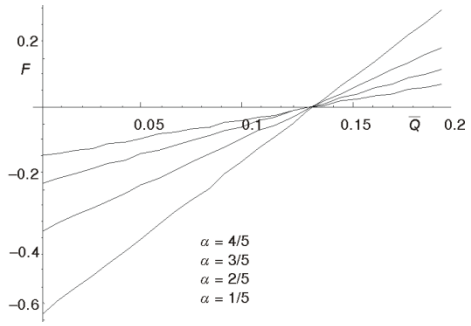

Figure 9. Friction force *vs.* averaged flow rate for various values of α at $\phi = 0.6$, $k = 1$, $t = 0.4$, $\beta = 4/5$, $\lambda_1 = 4$, $\lambda_2 = 1$, and $\lambda_3 = 1$

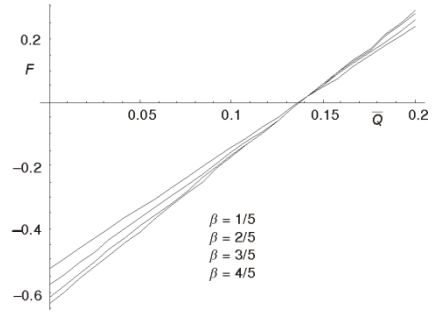

Figure 10. Friction force *vs.* averaged flow rate forvarious values of β at $\phi = 0.6$, $k = 1$, $t = 0.4$, $\alpha = 1/5$, $\lambda_1 = 4$, $\lambda_2 = 1$, and $\lambda_3 = 1$

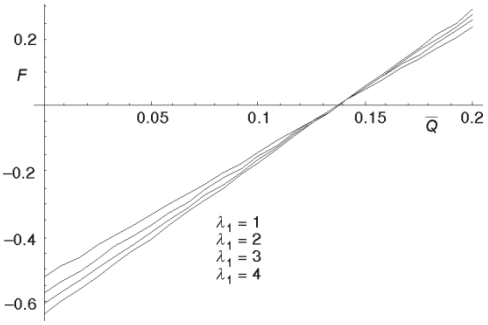

Figure 11. Friction force *vs.* averaged flow rate for various values of λ_1 at $\phi = 0.6$, $k = 1$, $t = 0.4$, $\alpha = 1/5$, $\beta = 4/5$, $\lambda_2 = 1$, and $\lambda_3 = 1$

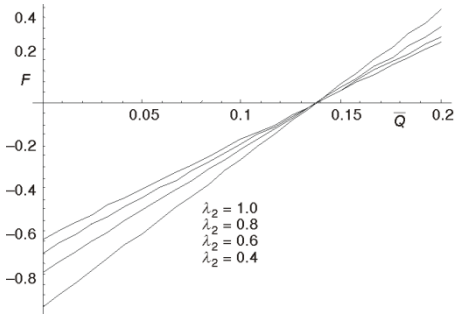

Figure 12. Friction force *vs.* averaged flow rate for various values of λ_2 at $\phi = 0.6$, $k = 1$, $t = 0.4$, $\alpha = 1/5$, $\beta = 4/5$, $\lambda_1 = 4$, and $\lambda_3 = 1$

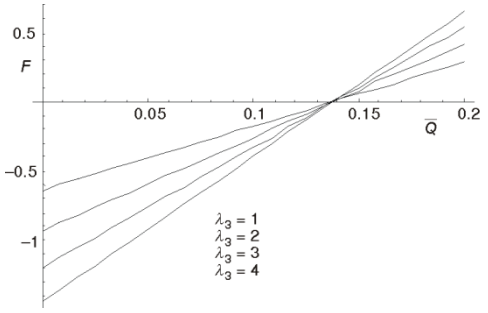

Figure 13. Friction force *vs.* averaged flow rate for various values of λ_3 at $\phi = 0.6$, $k = 1$, $t = 0.4$, $\alpha = 1/5$, $\beta = 4/5$, $\lambda_1 = 4$, and $\lambda_2 = 1$

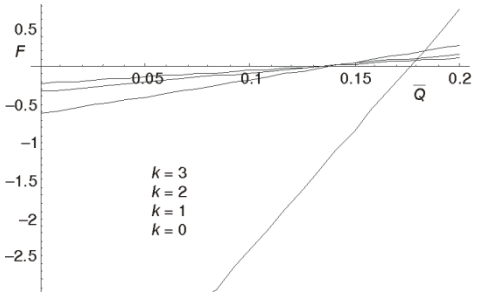

Figure 14. Friction force *vs.* averaged flow rate for various values of k at $\phi = 0.6$, $t = 0.4$, $\alpha = 1/5$, $\beta = 4/5$, $\lambda_1 = 4$, $\lambda_2 = 1$, ans $\lambda_3 = 1$

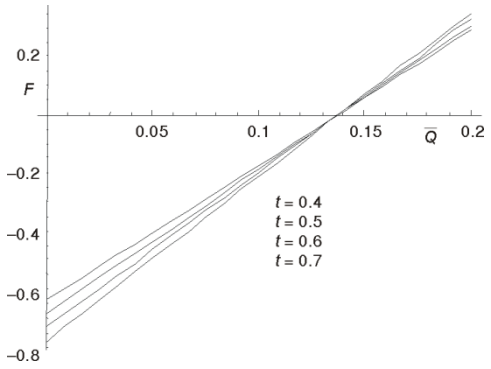

Figure 15. Friction force *vs.* averaged flow rate for various values of t at $\phi = 0.6$, $k = 1$, $\alpha = 1/5$, $\beta = 4/5$, $\lambda_1 = 4$, $\lambda_2 = 1$, and $\lambda_3 = 1$

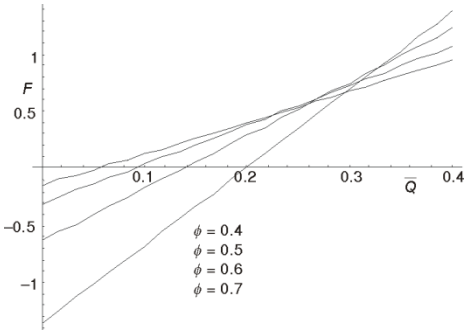

Figure 16. Friction force *vs.* averaged flow rate for various values of ϕ at $t = 0.4$, $k = 1$, $\alpha = 1/5$, $\beta = 4/5$, $\lambda_1 = 4$, $\lambda_2 = 1$, and $\lambda_3 = 1$

Figures 17-24 are illustrated in order to study the variations of Δp with $\bar{Q}$ for different fractional and ordinary models of fluids such as FBM ($\phi = 0.6$, $k = 1$, $t = 0.4$, $\alpha =$ $= 1/5$, $\beta = 4/5$, $\lambda_1 = 4$, $\lambda_2 = 0.1$, $\lambda_3 = 1$), BM ($\phi = 0.6$, $k = 1$, $t = 0.4$, $\alpha = 1$, $\beta = 1$, $\lambda_1 = 4$, $\lambda_2 = 0.1$, $\lambda_3 = 1$), FOBM ($\phi = 0.6$, $k = 1$, $t = 0.4$, $\alpha = 1/5$, $\beta = 4/5$, $\lambda_1 = 4$, $\lambda_2 = 0$, $\lambda_3 = 1$), OBM ($\phi = 0.6$, $k = 1$, $t = 0.4$, $\lambda_1 = 4$, $\lambda_2 = 0.1$, $\lambda_3 = 1$, $\alpha = 1$, $\beta = 1$), FMM ($\phi = 0.6$, $k = 1$, $t =$ $= 0.4$, $\alpha = 1/5$, $\beta = 4/5$, $\lambda_1 = 4$, $\lambda_2 = 0$, $\lambda_3 = 0$) MM ($\phi = 0.6$, $k = 1$, $t = 0.4$, $\alpha = 1$, $\beta = 1$, $\lambda_1 =$ $= 4$, $\lambda_2 = 0$, $\lambda_3 = 0$), FSGM ($\phi = 0.6$, $k = 1$, $t = 0.4$, $\alpha = 1/5$, $\beta = 4/5$, $\lambda_1 = 0$, $\lambda_2 = 0$, $\lambda_3 = 1$), and SGM ($\phi = 0.6$, $k = 1$, $t = 0.4$, $\alpha = 1$, $\beta = 1$, $\lambda_1 = 0$, $\lambda_2 = 0$, $\lambda_3 = 1$). It is observed that the pressure rise for standard models is more significant in comparison to their corresponding fractional models. Also it is seen that the sequence of increasing order of pressure rise for different fractional models as FOBM > FMM > FSGM > FBM. Similar observations are found for standard models of fluids such as OBM > MM > SGM > BM. Finally, the maximum pressure rise for OBM and minimum pressure rise for BM are noticed.

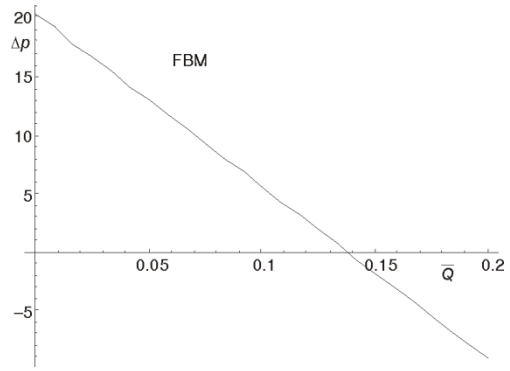

Figure 17. Pressure *vs.* averaged flow rate for FBM (ϕ = 0.6, k = 1, t = 0.4, α = 1/5, β = 4/5, λ_1 = 4, λ_2 = 0.1, and λ_3 = 1)

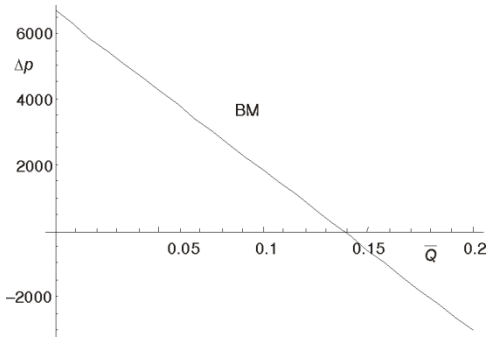

Figure 18. Pressure *vs.* averaged flow rate for BM (ϕ = 0.6, k = 1, t = 0.4, α = 1, β = 1, λ_1 = 4, λ_2 = 0.1, and λ_3 = 1)

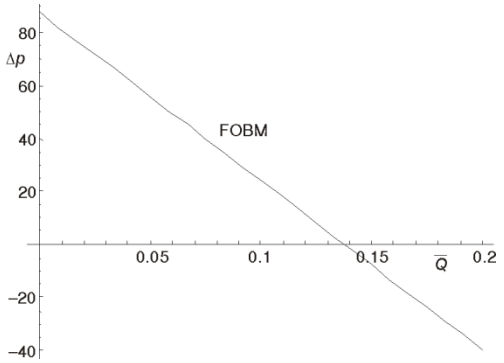

Figure 19. Pressure *vs.* averaged flow rate for FOBM (ϕ = 0.6, k = 1, t = 0.4, α = 1/5, β = 4/5, λ_1 = 4, λ_2 = 0, and λ_3 = 1)

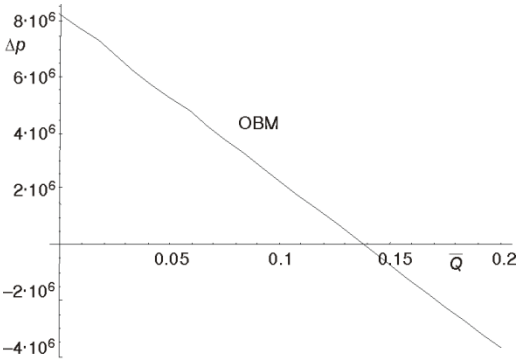

Figure 20. Pressure *vs.* averaged flow rate for OBM (ϕ = 0.6, k = 1, t = 0.4, α = 1, β = 1, λ_1 = 4, λ_2 = 0, and λ_3 = 1)

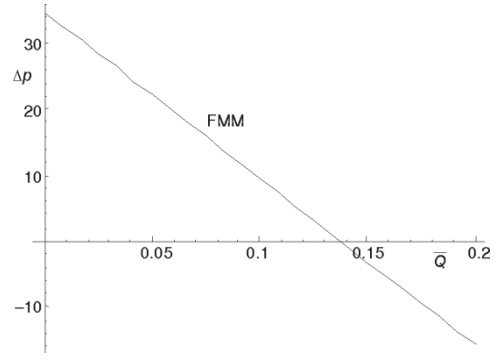

Figure 21. Pressure *vs.* averaged flow rate for FMM (ϕ = 0.6, k = 1, t = 0.4, α = 1/5, β = 4/5, λ_1 = 4, λ_2 = 0, and λ_3 = 0)

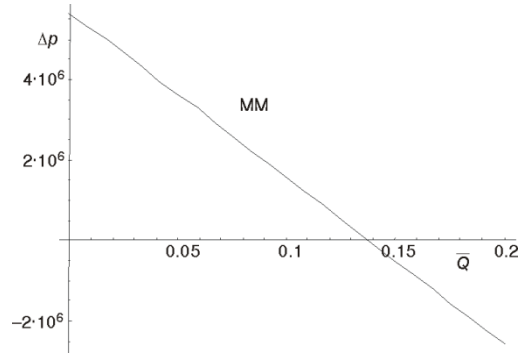

Figure 22. Pressure *vs.* averaged flow rate for MM (ϕ = 0.6, k = 1, t = 0.4, α = 1, β = 1, λ_1 = 4, λ_2 = 0, and λ_3 = 0)

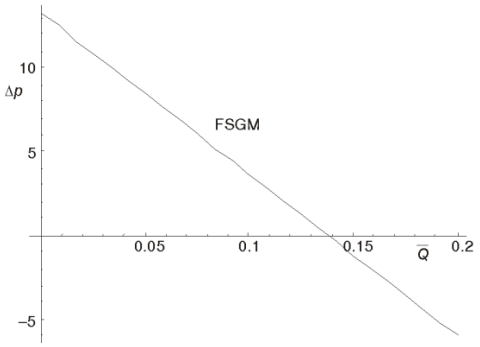

Figure 23. Pressure *vs.* averaged flow rate for FSGM (ϕ = 0.6, k = 1, t = 0.4, α = 1/5, β = 4/5, λ_1 = 0, λ_2 = 0, and λ_3 = 1)

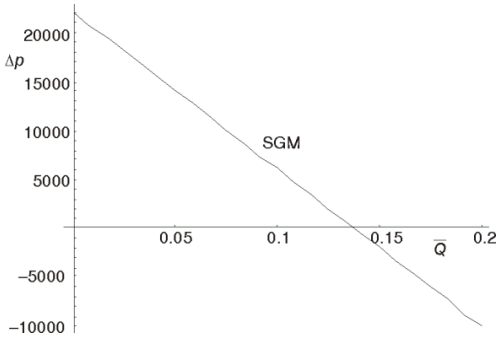

Figure 24. Pressure *vs.* averaged flow rate for SGM (ϕ = 0.6, k = 1, t = 0.4, α = 1, β = 1, λ_1 = 0, λ_2 = 0, and λ_3 = 1)

Concluding remarks

In this analysis, influence of wall slip condition on peristaltic flow of viscoelastic fluid with fractional Burgers' model under the long wavelength and low Reynolds number assumption through a channel has been discussed. Approximate analytical solutions have been obtained by homotopy analysis method. Interaction of various emerging parameters with peristaltic flow is studied with the help of illustrations. The comparison among the results of different models of fluids is made. On the basis of presented analysis, some interesting observations have been disclosed:

- pressure rise across one wavelength diminishes by increasing averaged flow rate,
- with the increase in α, the pressure rise decreases,
- the behavior of β on the pressure rise is opposite to that of α,
- pressure rise increases with increase in λ_1, λ_3, but increase in λ_2 reduces the pressure rise,
- the behavior of k on pressure rise is similar to that of α,
- an increase in ϕ increases the pressure rise and also similar character of t on pressure rise is pointed out,
- friction force has opposite character when compared with that of pressure rise,
- pressure rise for fractional models of the fluids is noted much lesser than that for the corresponding standard models, and
- the maximum pressure rise for OBM and minimum pressure rise for BM is remarkable.

Nomenclature

a – semi-width of the channel, [m]
c – wave velocity, [ms^{-1}]
F – friction force, [kgms^{-2}]
$\tilde{h}$ – transverse displacement of the wall, [m]
h – non-zero auxiliary parameter
k – slip parameters, [s]
$\tilde{p}$ – pressure, [kgm^{-1}s^{-2}]
Q – volume flow rate, [m^{3}s^{-1}]
$\tilde{S}$ – shear stress, [kgm^{-1}s^{-2}]
$\tilde{t}$ – time, [s]
$\tilde{u}$ – axial velocity, [ms^{-1}]
$\tilde{v}$ – transverse velocity, [ms^{-1}]

Greek symbols

$\dot{\gamma}$ – rate of shear strain, [radian]
$\tilde{\eta}$ – transverse co-ordinate [m]
λ – wavelength, [m]
$\tilde{\lambda}_1, \tilde{\lambda}_2, \tilde{\lambda}_3, \tilde{\lambda}_4$ – material constants, [s]
μ – viscosity, [kgm^{-1}s^{-1}]
$\tilde{\xi}$ – axial co-ordinate, [m]
ρ – fluid density, [kgm^{-3}]
$\tilde{\phi}$ – amplitude of the wave, [m]

References

[1] Latham, T. W., Fluid Motion in a Peristaltic Pump, M. Sc. thesis, MIT, Cambridge, UK, 1966
[2] Burns, J. C., Parkers, T., Peristaltic Motion, *J. Fluid Mech*., *29* (1967), 4, pp. 731-743
[3] Shapiro, A. H., Jafferin, M. Y., Weinberg, S. L., Peristaltic Pumping with Long Wavelengths at Low Reynolds Number, *J. Fluid Mech*., *37* (1969), 4, pp. 669-675
[4] Ebaid, A., Effects of Magnetic Field and Wall Slip Conditions on the Peristaltic Transport of a Newtonian Fluid in an Asymmetric Channel, *Physics Letters A*, *372* (2008), 24, pp. 4493-4499
[5] Ali, N., *et al*., Slip Effects on the Peristaltic Transport of MHD Fluid with Variable Viscosity, *Physics Letters A*, *372* (2008), 9, pp. 1477-1489
[6] Hayat, T., Qureshi, M. U., Ali, N., The Influence of Slip on the Peristaltic Motion of a Third Order Fluid in an Asymmetric Channel, *Physics Letters A*, *372* (2008), 15, pp. 2653-2664
[7] El-Shehawy, E. F., El-Dabe, N. T., El-Desoki, I. M., Slip Effects on the Peristaltic Flow of a Non-Newtonian Maxwellian Fluid, *Acta Mechanica*, *186* (2006), 1-4, pp. 141-159
[8] Tsiklauri, D., Beresnev, I., Non-Newtonian Effects in the Peristaltic Flow of a Maxwell Fluid, *Physical Review E*, *64* (2001), 3, pp.036303-036308
[9] Hayat, T., Ali, N., Asghar, S., Hall Effects on the Peristaltic Flow of a Maxwell Fluid in a Porous Medium, *Physics Letter A*, *363* (2007), 5-6, pp. 397-403
[10] Ali, N., Hayat, T., Asghar, S., Peristaltic Flow of a Maxwell Fluid in a Channel with Compliant Walls, *Chaos, Solitons and Fractals*, *39* (2009), 1, pp. 407-416
[11] Hayat, T., Ali, N., Peristaltic Motion of a Jeffrey Fluid Under the Effect of a Magnetic Field in a Tube, *Communication in Nonlinear Science and Numerical Simulation*, *13* (2008), 7, pp. 1343-1352
[12] Hayat, T., Ali, N., Asghar, S., Siddiqui, A. M., Exact Peristaltic Flow in Tubes with an Endoscope, *Applied Mathematics and Computation*, *182* (2006), 1, pp. 359-368
[13] Hayat, T., Ali, N., Asghar, S., An Analysis of Peristaltic Transport for Flow of a Jeffrey Fluid, *Acta Mechanica*, *193* (2007), 1-2, pp. 101-112
[14] Hayat, T., Nadeem, S., Asghar, S., Periodic Unidirectional Flows of a Viscoelastic Fluid with the Fractional Maxwell Model, *Applied Mathematics and Computation*, *151* (2004), 1, pp. 153-161
[15] Wenchang, T., Wenxiao, P., Mingyu, X., A Note on Unsteady Flows of a Viscoelastic Fluid with the Fractional Maxwell Model between Two Parallel Plates, *Int. J. of Non-Linear Mechanics*, *38* (2003), 5, pp. 645-650
[16] Wenchang, T., Mingyu, X., Plane Surface Suddenly Set in Motion in a Viscoelastic Fluid with Fractional Maxwell Model, *Acta Mechanica Sinica*, *18* (2002), 4, pp. 342-349
[17] Friedrich, C., Relaxation and Retardation Functions of the Maxwell Model with Fractional Derivatives, *Rheologica Acta*, *30* (1991), 2, pp. 151-158
[18] Qi, H., Jin, H., Unsteady Rotating Flows of a Viscoelastic Fluid with the Fractional Maxwell Model between Coaxial Cylinders, *Acta Mechanica Sinica*, *22* (2006), 4, pp. 301-305
[19] Qi, H., Xu, M., Unsteady Flow of Viscoelastic Fluid with Fractional Maxwell Model in Channel, *Mechanics Research Communications*, *34* (2007), 2, pp. 210-212
[20] Khan, M., *et al*., Decay of Potential Vortex for a Viscoelastic Fluid with Fractional Maxwell Model, *Applied Mathematical Modelling*, *33* (2009), 5, pp. 2526-2533
[21] Vieru, D., Fetecau, C., Fetecau, C., Flow of a Viscoelastic Fluid with the Fractional Maxwell Model between Two Side Walls Perpendicular to a Plate, *Applied Mathematics and Computation*, *200* (2008), 1, pp. 459-464
[22] Mahmood, A., *et al*., Exact Analytic Solutions for the Unsteady Flow of a Non-Newtonian Fluid between Two Cylinders with Fractional Derivative Model, *Communication in Nonlinear Science and Numerical Simulation*, *14* (2009), 8, pp. 3309-3319
[23] Wang, S., Xu, M., Axial Couette Flow of Two Kinds of Fractional Viscoelastic Fluids in an Annulus, *Nonlinear Analysis, Real World Applications*, *10* (2009), 2, pp. 1087-1096
[24] Khan, M., Ali, S. H., Qi, H., On Accelerated Flows of a Viscoelastic Fluid with the Fractional Burgers' Model, *Nonlinear Analysis, Real World Applications*, *10* (2009), 4, pp. 2286-2296
[25] Qi, H., Xu, M., Some Unsteady Unidirectional Flows of a Generalized Oldroyd-B Fluidwith Fractional Derivative, *Applied Math. Modelling*, *33* (2009), 11, pp. 4184-4191
[26] Qi, H., Xu, M., Stokes' First Problem for a Viscoelastic Fluid with the Generalized Oldroyd-B Model, *Acta Mech Sinica*, *23* (2007), 5, pp. 463-469

[27] Nadeem, S., General Periodic Flows of Fractional Oldroyd-B Fluid for an Edge, *Physics Letters A*, *368* (2007), 3-4, pp. 181-187
[28] Hayat, T., Khan, M., Asghar, S., On the MHD Flow of Fractional Generalized Burgers' Fluid with Modified Darcy's Law, *Acta Mech Sinica, 23* (2007), 3, pp. 257-261
[29] Liao, S. J., Homotopy Analysis Method, A New Analytic Method for Nonlinear Problems, *Applied Mathematics and Mechanics, 19* (1998), 10, pp. 957-962
[30] Liao, S. J., On the Proposed Homotopy Analysis Technique for Nonlinear Problems and Its Applications, Ph. D. thesis, S. Jiao Tong University, Shanghai, China, 1992
[31] Das, S., Gupta, P. K., Application of Homotopy Perturbation Method and Homotopy Analysis Method to Fractional Vibration Equation, *International Journal of Computer Mathematics, 88* (2011), 2, pp. 430-441
[32] Das, S., Gupta, P. K., Homotopy Analysis Method for Solving Fractional Hyperbolic Partial Differential Equations, *International Journal of Computer Mathematics*, *88* (2011), 3, pp. 578-588
[33] Hayat, T., Khan, M., Asghar, S., Magneto Hydrodynamic Flow of an Oldroyd 6-Constant Fluid, *Applied Mathematics and Computation, 155* (2004), 2, pp. 417-425
[34] Liao, S. J., An Analytical Solution of Unsteady Boundary Layer Flows Caused by an Impulsively Stretching Plate. *Comm. in Nonlinear Sci. and Numerical Simulation*, *11* (2006), 3, pp. 326-339
[35] Wu, W., Liao, S. J., Solving Solitary Waves with Discontinuity by Means of the Homotopy Analysis Method, *Chaos, Solitons and Fractals, 26* (2005), 1, pp. 177-185
[36] Liao, S. J., Beyond Perturbation: Introduction to the Homotopy Analysis Method, Chapman and Hall, CRC Press, Boca Ration, Fla., USA, 2003
[37] Abbaoui, K., Cherruault, Y., New Ideas for Proving Convergence of Decom-Position Methods, *Comp. & Mathe. with Applications, 29* (1995), 7, pp. 103-108

Paper submitted: September 24, 2009
Paper revised: February 14, 2010
Paper accepted: April 14, 2010